

A magneto-motive ultrasound platform designed for pre-clinical and clinical applications

Diego Ronaldo Thomaz Sampaio*, Felipe Wilker Grillo, Alexandre Colello Bruno, Theo Zeferino Pavan, Antonio Adilton Oliveira Carneiro

Abstract Introduction: Magneto-motive ultrasound (MMUS) combines magnetism and ultrasound (US) to detect magnetic nanoparticles in soft tissues. One type of MMUS called shear-wave dispersion magneto-motive ultrasound (SDMMUS) analyzes magnetically induced shear waves (SW) to quantify the elasticity and viscosity of the medium. The lack of an established presets or protocols for pre-clinical and clinical studies currently limits the use of MMUS techniques in the clinical setting. **Methods:** This paper proposes a platform to acquire, process, and analyze MMUS and SDMMUS data integrated with a clinical ultrasound equipment. For this purpose, we developed an easy-to-use graphical user interface, written in C++/Qt4, to create an MMUS pulse sequence and collect the ultrasonic data. We designed a graphic interface written in MATLAB to process, display, and analyze the MMUS images. To exemplify how useful the platform is, we conducted two experiments, namely (i) MMUS imaging to detect magnetic particles in the stomach of a rat, and (ii) SDMMUS to estimate the viscoelasticity of a tissue-mimicking phantom containing a spherical target of ferrite. **Results:** The developed software proved to be an easy-to-use platform to automate the acquisition of MMUS/SDMMUS data and image processing. In an *in vivo* experiment, the MMUS technique detected an area of $6.32 \pm 1.32 \text{ mm}^2$ where magnetic particles were heterogeneously distributed in the stomach of the rat. The SDMMUS method gave elasticity and viscosity values of $5.05 \pm 0.18 \text{ kPa}$ and $2.01 \pm 0.09 \text{ Pa.s}$, respectively, for a tissue-mimicking phantom. **Conclusion:** Implementation of an MMUS platform with addressed presets and protocols provides a step toward the clinical implementation of MMUS imaging equipment. This platform may help to localize magnetic particles and quantify the elasticity and viscosity of soft tissues, paving a way for its use in pre-clinical and clinical studies.

Keywords: Ultrasound, Magneto-motive ultrasound, Shear wave, Elastography, Magnetic nanoparticles.

Introduction

Magneto-motive ultrasound (MMUS) has been used to localize magnetic nanoparticles within soft tissues, and allows the generation of ultrasound-based molecular imaging. Most of the nanoparticles are weak contrast agents to ultrasound, including magnetic nanoparticles. MMUS can overcome this issue by detecting the motion induced by the interaction between an external magnetic field and the magnetic nanoparticles as ultrasonic echoes (Oh et al., 2006). A continuous-time harmonic magnetic field with frequency in order of few Hertz, or a burst of magnetic field pulses, usually excites the magnetic nanoparticles (Mehrmohammadi et al., 2011c). Using this technique researchers have also investigated MMUS to evaluate the viscoelasticity of soft tissues by tracking the shear waves induced by motion of the magnetic nanoparticles (Almeida et al., 2014; 2015; Pavan et al., 2012), a method known as shear-wave dispersion magneto-motive ultrasound

(SDMMUS) (Almeida et al., 2014). The velocity and attenuation of the shear waves can be analyzed to obtain the elasticity and viscosity of the medium (Zhao et al., 2010).

In MMUS and SDMMUS, the ultrasound system needs a high frame rate to capture the induced harmonic motion and shear waves. Enhanced hardware systems are costly (Jensen et al., 2013; Kaczkowski and Daigle, 2011), but they could provide real-time MMUS imaging. Some clinical ultrasound equipment provide a graphical user interface, called ultrasound research interface (URI) (Wilson et al., 2006). This research interface can be configured to collect radiofrequency (RF) data at high frame rates ($>1 \text{ kHz}$), which can be processed by applying a speckle-tracking algorithm (Viola and Walker, 2005; Zahiri-Azar et al., 2010) to monitor motion with frequencies in the order of hundreds of hertz (Sarvazyan et al., 2013). Unfortunately, the commercial URI systems are expensive, limited, or not

*e-mail: diegorts@usp.br

flexible enough to evaluate and test novel ultrasound techniques. Efforts have focused on incorporating software interfaces in the commercial ultrasound equipment (Hemmsen et al., 2012; Shamdasani et al., 2008) to facilitate the implementation of new techniques, such as 2-D temperature imaging and vibro-acustography. This strategy could provide a more accessible and available platform for clinical application (Liu and Ebbini, 2010; Urban et al., 2011).

Despite the various applications of MMUS, there has been little attention in its implementation in the clinical setting. Successful implementation of MMUS and SDMMUS can provide new opportunities for clinical applications of ultrasound imaging, such as localization of brachytherapy seeds (McAleavey et al., 2003), monitoring of stomach emptying (Bruno et al., 2015), estimation of tissue viscoelasticity (Almeida et al., 2015) and molecular imaging (Evertsson et al., 2014). Moreover, combining photoacoustics with MMUS can also help to improve the sensitivity of the technique to detect multifunctional nanoparticles with multiple contrast mechanisms (Jin et al., 2010; Qu et al., 2011).

This study aimed to develop a more practical MMUS platform for application in pre-clinical and clinical trials. We present a new platform dedicated to the MMUS technique based on a software for data acquisition (MMUS-A) and another software for image processing (MMUS-PA). We have explored the MMUS technique to achieve dedicated pulse sequences, and we have created an optimized configuration to acquire and process the RF data. We have characterized the developed platform through an SDMMUS experiment and obtained the mechanical properties of a tissue-mimicking phantom; we have also conducted an *in vivo* study to localize magnetic particles in the stomach of a rat. The developed system relies on a protocol that is compatible with most of the clinical ultrasound systems, paving the way for the use of MMUS in the clinical setting.

Methods

Laboratory system overview

Figure 1a shows a diagram of a typical MMUS laboratory system. Our system consisted of a dual-channel waveform generator (33522a, Agilent, California, USA), an audio power amplifier (5000W - Dynamic 20.000 Ω , Ciclotron, Brazil) connected to a solenoid (coil) to generate the magnetic field, and a clinical ultrasound equipment (Sonix RP, Ultrasonix, Canada). The waveform generator was connected to the ultrasound equipment via universal serial bus (USB) to synchronize the pulse-eco sequence with the magnetic field generated by the coil. Two ultrasonic

probes (L14-5/38; EC9-5/10, Ultrasonix, Canada) with central frequencies of 7.2 MHz and 6.5 MHz were used.

A user interface called MMUS-A was developed in Visual Studio Express 2010 (Microsoft, USA) with C++ and Qt4 (Digia, Finland). The software development kit: IVI-COM 1.0.1 (IVI Foundation, USA) and Texo 5.7.4 (Ultrasonix, Canada) provide the capability to control both the ultrasound equipment and waveform generator. Qt4 provides classes to create threads, images, and network (Qt, 2016), which were used to create an abstraction presented by an object-oriented environment with the functionalities depicted in Figure 1b. The blue box in Figure 1b highlights the editable functionalities of the user interface and generates a synchronized pulse sequence for MMUS. The white box highlights the software function that shows real-time B-mode images and transfers the acquired data through a Transmission Control Protocol/Internet Protocol (TCP/IP) cable connected to an external personal computer (PC). Figure 1c illustrates the final user interface.

Design of the pulse sequence

The MMUS pulse sequence was implemented by combining a synchronized beamforming pulse-echo with a magnetic field burst. Pulsed MMUS is more desirable than continuous MMUS to avoid coil heating (Mehrmohammadi et al., 2011a). Thus, user can define the settings that include the ultrasonic beamforming parameters, the magnetic field shape (e.g., sinusoidal), the magnetic field frequency f_B , and the excitation duration T_B to allow automated acquisition.

The high frame rate (HFR) sub-sector method (Zahiri-Azar et al., 2010) is a pulse-echo beamforming technique that was implemented by emitting ultrasound waves from all the available channels; which are 128 transmitting channels. Then, a delay-and-sum algorithm was applied. The frame rate f_r is inversely proportional to the number of received scanlines and the number of scanlines determines the size of a sector (Cobbold, 2006). Therefore, HFR beamforming overcomes frame rate limitations in the clinical hardware by creating sub-sectors containing fewer scanlines than the full sector. Then, the data corresponding to each sub-sector are concatenated into a full sector (Zahiri-Azar et al., 2010). According to the HFR method, the number of sub-sectors increases the total duration of an acquisition proportionally, raising the number of emissions.

The interaction between magnetic particles and the magnetic field lead the magnetic force F_B to be twofold the value of the magnetic field frequency $f_{F_B} = 2f_B$ (Colello Bruno et al., 2013; Mehrmohammadi et al.,

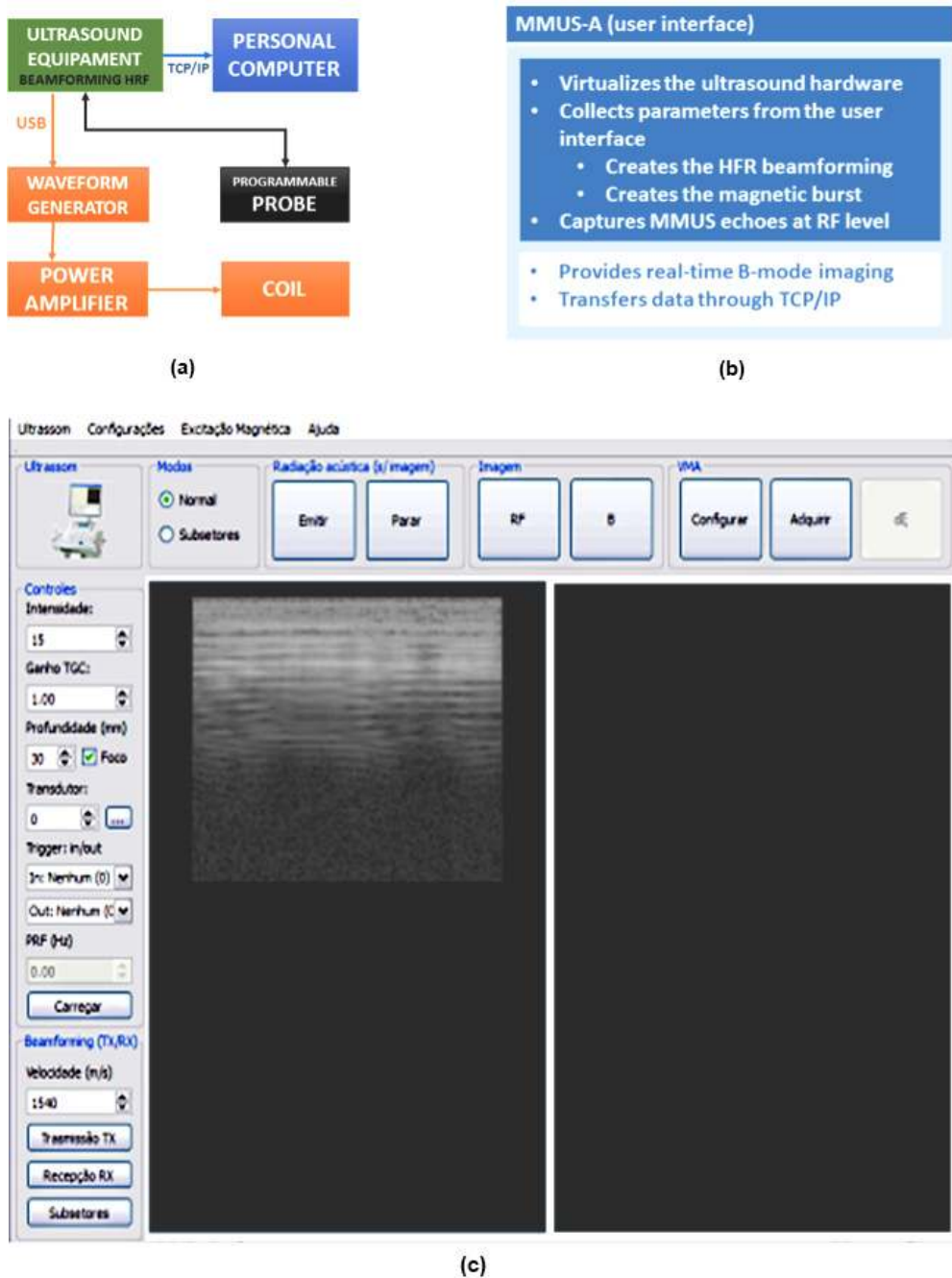


Figure 1. Diagram of a typical MMUS laboratory system. (a) The clinical ultrasound equipment with a programmable linear array probe is connected to a waveform generator via USB connection. The waveform is amplified to deliver current to the coil, which is used to generate the magnetic flux; (b) The user interface of MMUS-A is an easy-to-use interface that provides functionalities to create automated acquisition of MMUS data; (c) The main window and dialogs of MMUS-A permits online B-mode acquisition and transmission of MMUS data.

2011b; Oh et al., 2006). Hence, according to the Nyquist theorem, f_r has to be greater than $2f_{F_B}$. This condition is essential to visualize the magnetically induced motion during magnetic excitation (Oh et al., 2006), without aliasing artifacts. The pulse sequence was designed to fit all those requirements.

The pulse-echo mode and the magnetic excitation are turned on simultaneously. The magnetic field is applied during the ultrasonic scan time T_{US} with a duration of T_B , which must be less than or equal to T_{US} , ensuring the synchronism between subsequent sub-sectors. The MMUS pulse sequence was repeated

20 times (each sub-sector was composed of 5% of the total number of scanlines in the full sector) to cover 100% of the sector as follows:

1. The ultrasound scan and magnetic excitation were turned on;
2. After T_b the magnetic excitation was turned off;
3. The ultrasound scan was turned off, and then sub-sectors acquired during T_{US} were stored;
4. The next sub-sector i^{th} was acquired according to steps 1 to 3;
5. Steps 1 to 4 were repeated at a repetition frequency of $\frac{1}{T_{US}}$ to cover 100% of the sector;
6. After step 5, the sub-sectors were concatenated, stored into a HFR cinelooop, and transferred to the PC.

We defined a group of default values, organized as presets, to help to automate the MMUS and SDMMUS experiments. The frame rate was set to 2000 Hz, at an axial depth of acquisition of 90 mm, by creating sub-sectors containing 5% (2 mm) of the total number of elements of the linear transducer (~40 mm) full sector. A sampling frequency of 40 MHz was used to capture the RF data, which can be processed to obtain displacements in the order of a few microns (Viola and Walker, 2005). The magnetic pulses were calibrated and defined as a burst of sinusoidal cycles with frequency in the range of tens to hundreds of hertz, which was limited to a quarter of the Nyquist frequency. Table 1 summarizes the presets used in the experiments.

MMUS images generation

The RF data was processed by applying a motion tracking cross-correlation algorithm. The algorithm compared consecutive RF echoes that were axially displaced by the action of the magnetic force, to give

the speckle time-delay (lag) in the pulse-echo axial direction. With this algorithm, magnetically induced motion was obtained over a region by using pairs of windowed RF echoes that were acquired under different instants of time. The size of the windows, given in millimeters, and the distance of adjacent windows (% of overlap) are the most important parameters of motion tracking in terms of spatial resolution (Viola and Walker, 2005).

For a single element of the probe, a pair of consecutive scanlines was divided into overlapping windows by using a 1D rectangular window of 2 mm with a 50% overlap. Lagrange interpolation was applied around the maximum peak of the cross-correlation signal to obtain the motion between two consecutive RF echoes (Viola and Walker, 2005; Zahiri-Azar and Salcudean, 2006). The algorithm was repeated for each element of the probe to generate an MMUS particle motion image M_u . This image enabled visualization of the motion at each spatial location of the acquisition depth or a predefined region. The intensity of M_u was adjusted to meters by dividing its value by twice the sampling frequency of ultrasound machine and then multiplying the result by the speed of sound, e.g., 1540 m/s (Cobbold, 2006). The MMUS particle velocity image M_v , was the time derivative of M_u , which was obtained in the time interval

$\Delta t = \frac{1}{fr}$, giving the dimension of meters per second:

$$M_v = \left| \frac{d}{dt} M_u(t + \Delta t) \right|_{\Delta t = \frac{1}{fr}} \cong \frac{\Delta M_u}{\Delta t} = \Delta M_u \times fr \quad (1)$$

All the aforementioned details of motion tracking were implemented in MMUS-PA, a platform that is used to obtain images and analyze motion. Figure 2 shows MMUS-PA, developed using MATLAB 2014a (MathWorks, USA) to display the offline B-mode, MMUS images, and the spectral analysis.

Experiments

Two experiments, namely (i) *in vivo* experiment and (ii) an experiment using a phantom, were conducted to exemplify how useful the platform is. The *in vivo* experiment involved detection of magnetic particles in the stomach of a rat. The phantom study was developed to estimate the elasticity and viscosity of the phantom by using SDMMUS.

We used the MMUS system described in the previous section to collect the data. The magnetizing field setup was calibrated to deliver a maximum magnetic field in the region of interest. For the phantom measurements, a cylindrical magnetic core of ferrite was used as a flux concentrator. All the experiments were conducted at room temperature of

Table 1. Default magnetic and ultrasonic instructions (preset) used in the MMUS experiments.

Default preset configuration	
Parameter	Value
Acquisition depth (mm)	30-90
Ultrasound frequency (MHz)	5-12
Ultrasound sampling frequency (MHz)	40
Frame rate (Hz)	2000
Magnetic waveform shape	Sinusoidal burst
Magnetic frequency (Hz)	35-150
Duration of magnetic burst in number of cycles	1-5

24 °C. The MMUS pulse sequence was configured according to the preset shown in Table 1.

i) *In vivo*: animal handling and image analysis

In the *in vivo* study (Colello Bruno et al., 2014), we used a gavage needle to deliver ferrite particles (TH 50, Thornton Electronics, Brazil) of 50 μm average size, mixed in yogurt (Chandelle, Nestle, Switzerland) at a mass concentration of 10% directly in the stomach of a male Wistar rat (approximate weight of 300 g). An ultrasound microconvex probe (model EC9-5/10, Ultrasonix, Canada) was placed in the coil, as illustrated in Figure 3a. The ultrasound transducer focus and the magnetic field were positioned over the stomach

region of the rat (Figure 3a). The MUS RF data were acquired right after the gavage procedure. The coil (with the height of 14 mm, outer diameter of 92 mm, and inner diameter of 48 mm) was driven at 35 Hz with current amplitude of 1 A, to provide a peak of magnetic field of 5 mT at 50 mm away from the coil. Before the experiment, the rat was anesthetized with chloral hydrate 4% and had the abdomen shaved to improve acoustic coupling. The local Animal Ethics Committee approved all the procedures. For a more detailed description of this experiment, the reader is referred to (Colello Bruno et al., 2014).

We analyzed the MMUS images after defining a region of interest (ROI), where the magnetic force induced the highest displacements with a frequency

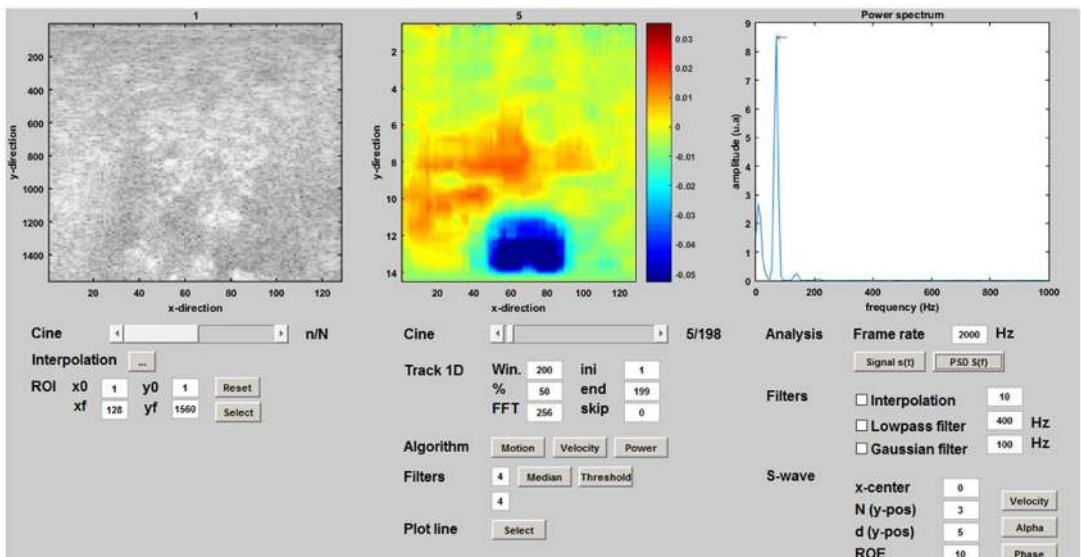


Figure 2. MMUS-PA interface. From left to right examples of B-mode image, MMUS image, and spectral density are displayed. The maximum peak from the spectral density to indicate the frequency of the MMUS motion.

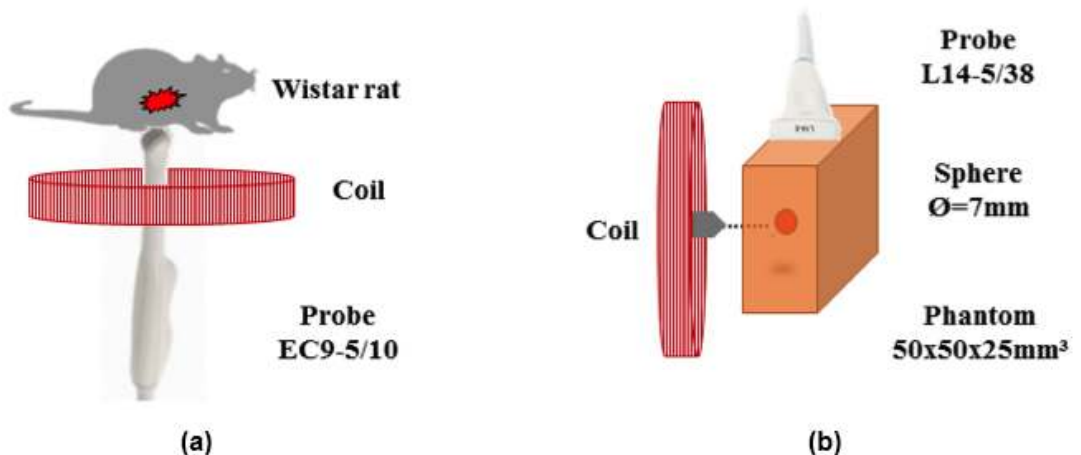


Figure 3. Illustration of (a) the *in vivo* experiment, which used a magnetizing coil around the micro convex probe; and (b) the phantom experiment, which used an external magnetizing coil to generate magnetically induced shear wave.

f_{FB} . For that, we analyzed thresholds between 5% and 95% of the highest relative energy of the particle velocity signal, which was used to generate a mask for locating and segmenting ROI precisely. This relative energy was estimated by the sum of square of the particle velocity signal.

ii) Phantom: production and analysis of shear wave

The *phantom* study, based on (Pavan et al., 2012), was designed to induce shear waves due to the magnetic excitation. For this purpose, a rectangular phantom ($50 \times 50 \times 25$ mm) made of paraffin-gel wax was prepared according to the procedure described in (Vieira et al., 2013). A spherical inclusion with a diameter of 7 mm, containing ferrite at a 50% mass concentration, was positioned inside the phantom. The coil (with the height of 22 mm, inner diameter of 45 mm, and outer diameter of 89 mm) was positioned near the phantom, so that the tip of the ferrite core was aligned with the sphere and positioned at a distance of 1 mm away from the surface of the phantom (see Figure 3b). At this distance from the coil, a magnetic field with amplitude of 300 mT was generated synchronized with the ultrasound scan; both the magnetic excitation and the ultrasonic scan were gated by MMUS-A (see section “Design of the pulse sequence”). An ultrasound linear probe (model L14-5/38, Ultrasonix, Canada) was placed on the top of the phantom, perpendicularly to the axis of the coil, as depicted in Figure 3b.

The motion created by action of the magnetic force in the region of excitation (ROE) at time t_0 and depth of y_0 generated a shear wave that propagated through the phantom with group velocity c_g . To obtain the group velocity of shear wave in the distance interval of y_0 and y , the time delay $\Delta t = t - t_0$ between two time

signals was estimated by using cross-correlation. The distance $\Delta y = y - y_0$ divided by the time interval Δt gave the group velocity:

$$c_g = \frac{\Delta y}{\Delta t}. \quad (2)$$

After estimating the group velocity, we applied a Gaussian filter to the signal of the shear wave and selected a 50% bandwidth at f_{sw} . Then, we assumed that the SW signal was monochromatic during the analysis which gives the attenuation coefficient α according to:

$$A(y) = e^{-\alpha y} \quad (3)$$

In addition, we unwrapped the phase change ϕ along the axial direction y to estimate the phase velocity c_p (Parolai, 2009):

$$c_p = 2\pi f_{sw} \frac{\Delta y}{\Delta \phi} \quad (4)$$

All the parameters (i.e., group velocity, phase velocity, and attenuation coefficient) were determined by using 10 experimental points obtained at different depths. c_g and c_p were obtained by fitting a linear polynomial to the curves $(\Delta y, \Delta t)$ and $(\Delta \phi, \Delta t)$, respectively. The amplitude decay was adjusted to exponential curve to obtain α . In addition, we calculated the R-squared value for each curve to indicate the model quality.

Results

Figure 4 shows the results obtained for the *in vivo* experiment. Figure 4a corresponds to a rat B-mode image overlaid with the MMUS image (red area), indicating the region where the maximum velocity of the particle was 4.0 mm/s. We determined this

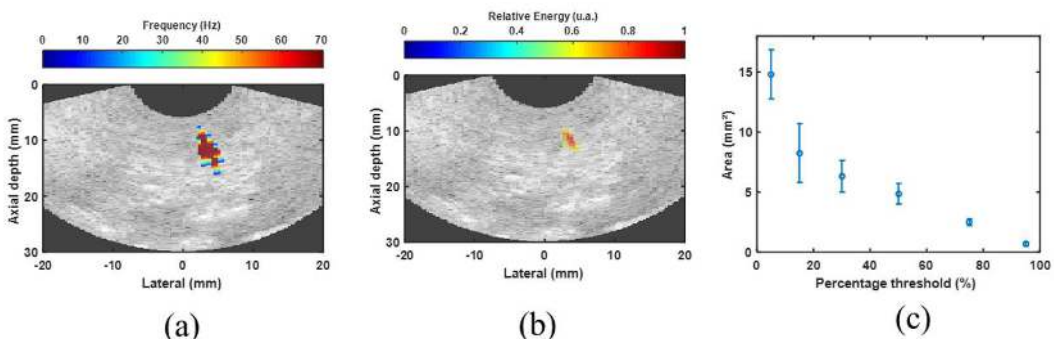


Figure 4. Results for the localization of the magnetic particles inside the stomach of the rat. (a) The MMUS image (red area) highlighting a motion of 70 Hz; (b) A small region localized by using the relative energy threshold percentage of 50%; (c) Area estimated by using ellipsoid segmentation and different threshold percentages of the maximum relative energy.

MMUS image region by detecting the region where the movements had a frequency of 70 ± 1 Hz. In Figure 4b, the same B-mode image is overlaid with the relative energy of the motion shown in Figure 4a. Also, we obtained the ROI area in Figure 4b by using a threshold percentage of 50% of the maximum relative energy, which presents a smaller area (see Figure 4b) than the region shown in Figure 4a. We varied the threshold percentage between 5% and 95% of the maximum relative energy to measure the ROI area, the area calculated by using an ellipsoid approximation (Figure 4c). We estimated areas of 8.25 ± 2.45 mm², 6.32 ± 1.32 mm², 4.85 ± 1.06 mm², and 2.48 ± 0.28 mm² for the threshold percentages of 15%, 30%, 50%, and 95%, respectively.

Figure 5 displays the results of the SDMMUS phantom experiment. Figure 5a contains a phantom B-mode image overlaid with the MMUS image (red area) indicating the region where the sphere was moved by an oscillating magnetic field in the frequency of 100 Hz with a duration of one cycle ($T_B = 10$ ms). Figure 5b shows an image of MMUS M_v versus time of a scanline at the lateral position of 1 mm (see Figure 5a) and depicts the propagation of shear wave for $T_{US} = 50$ ms.

The ferrite sphere corresponded to the ROE area localized between the axial depths of 35 mm and 45 mm with a cross-section area of 38.48 mm². When we used a percentage threshold of 30%, we estimated the ROE area as 42.14 ± 2.79 mm². After the magnetic excitation at $f_B = 100$ Hz a shear wave, identified by the arrow shown in Figure 5b, propagated from the ROE and reached the top of the phantom 15 ms after the beginning of the magnetic excitation. After that, the reflections emerged from the phantom/probe interface (in the region from 0 mm to 10 mm of axial depth) in the M_v image. We obtained the power spectrum of the time signal for depths of 25 mm, final SW (SWf), 35 mm, initial SW (SWi), and 40 mm (ROE). Then, each time signal was split into two 10 ms time-window which provided the spectral information about excitation (from 0 to 10 ms) and SW propagation (from 10 to 20 ms), as shown in Figure 5c. The peak frequencies of these three signals were different (Figure 5c). We believe this shift in frequency is due to the viscoelastic behavior of the paraffin gel, which acts as a dispersive medium and attenuates higher shear wave frequencies.

Figure 6 shows the images of MMUS M_v at 10 ms (6a), 15 ms (6b), and 20 ms (6c) after the beginning

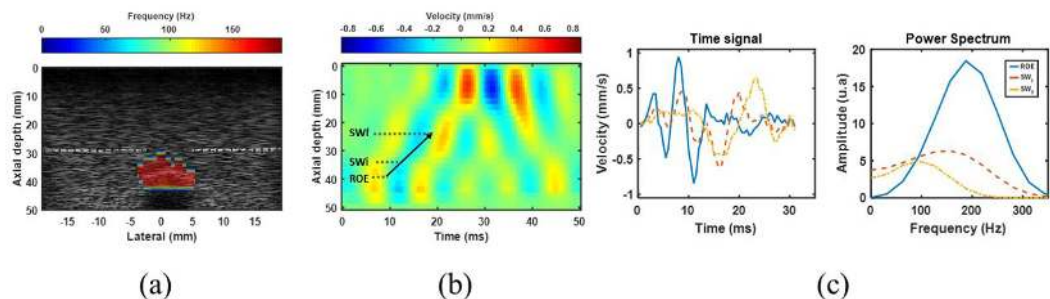


Figure 5. (a) B-mode image overlaid with MMUS image shows a solid ferrite sphere moving in a frequency of 200 Hz within a paraffin phantom. A single pulse of magnetic field with frequency of 100 Hz moved the sphere; (b) M_v versus time of a scanline at the lateral position of 1 mm. The movement inside ROE generated a shear wave, which propagated from 35 mm (dashed-SWi) to 25 mm (dashed-SWf) of depth; (c) The power spectrum of a time window of 10 ms of the time signal at depths of 25 mm (SWf – dash-dot), 35 mm (SWi – dash), and 40 mm (ROE), respectively.

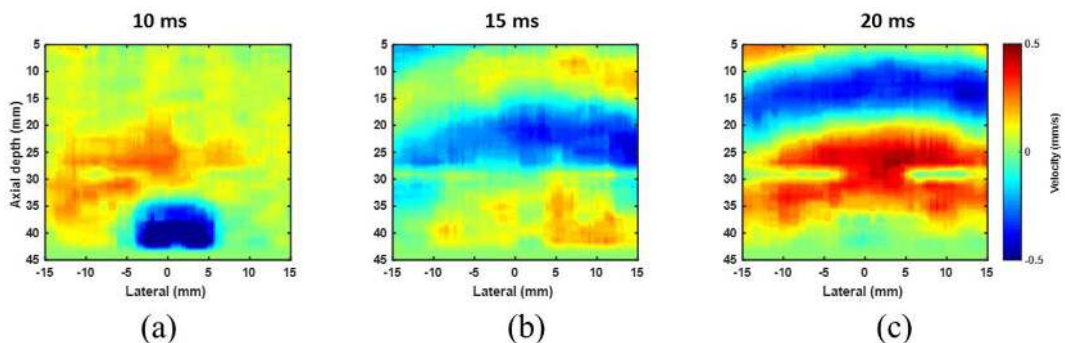


Figure 6. Shear wave propagating through the phantom after applying a magnetizing field of 100 Hz for (a) 10 ms; (b) 15 ms; and (c) 20 ms by. The scale was fixed at -0.5 to 0.5 mm/s.

of the magnetic excitation. These images were spatial representations, at fixed times, of the propagation of shear wave shown in Figure 5b. We estimated c_g by choosing a time interval between 10 ms to 20 ms and a total distance of 10 mm (from a depth of acquisition in 25 mm to 35 mm).

Moreover, we applied a Gaussian filter with center frequency of 100 Hz and 50% bandwidth to provide the shear wave with a monochromatic signal to allow estimation of α and c_p at 100 Hz. The group velocity, the attenuation coefficient, and the phase velocity were $c_g = 4.17 \pm 0.74$ m/s, $\alpha = 70.65$ Neper/m, and $c_p = 2.88 \pm 0.07$ m/s, respectively. Finally, elasticity and viscosity, quantified with the Kelvin-Voigt model (Zhao et al., 2010), were 5.05 ± 0.18 kPa and 2.01 ± 0.09 Pa.s, respectively.

Discussion

Previous studies have reported on the applicability of MMUS and SDMMUS to obtain important information about soft tissues. However, these studies did not focus on the implementation of MMUS in clinical ultrasound scanners (Evertsson et al., 2014; Mehrmohammadi et al., 2011c; Oh et al., 2006).

The present paper shows that the clinical ultrasound equipment are able to control MMUS magnetic excitation synchronized with ultrasound imaging. Moreover, synchronization with the software-controlled platform clearly is a more practical approach to MMUS imaging. As proposed here, it is possible to employ distinct probes to combine a setup that uses the ultrasound equipment to control all the MMUS acquisition parameters with the B-mode in a clinical setting. Reported results here, show that the linear array and the convex array can be placed in different positions not affecting the generation of MMUS images which attest the viability of MMUS in a clinical environment.

The motion-tracking algorithm (Viola and Walker, 2005) can be used at a fixed window size of 2 mm and 50% overlap to give MMUS images with axial resolution of almost 1 mm. In this case, the minimum detectable amplitude is limited by the standard deviation of the motion-tracking algorithm, which is around 0.04 mm/s in the present case. In addition, our MATLAB 2014a program takes 20 seconds to process a cineloop that lasts 100 ms with a PC (i7@2.60GHz, 12GB DDR3). Analysis of the images provides a good estimation of the ROI area and helps calculation of the mechanical parameters of soft tissues. However, in the latter a variation in the proportion of the overlap, to generate M_v , can change the velocity and attenuation of SW. In addition, an R-square value higher than

0.95 is essential to make the estimated elasticity and viscosity more reliable.

The depth of acquisition (30 mm to 90 mm) of the default used preset here is adequate for most applications, including phantom and pre-clinical studies (Almeida et al., 2015; Colello Bruno et al., 2014). Here, the depth is limited to 30 mm because a minimal propagation path of 10 mm is necessary to estimate the attenuation and velocity of the shear wave by using Equations 2, 3, and 4 (Deffieux et al., 2009).

A magnetic field with a few number of cycles and below a frequency limit of $f_B = 150$ Hz (see Table 1) is sufficient for MMUS and SDMMUS to prevent the coil heating (Mehrmohammadi et al., 2011a). Therefore, our MMUS pulse sequence satisfies the Nyquist restriction with a frame rate ~ 6.5 times of the Nyquist frequency and it doesn't require a frame rate above 2000 Hz. These values can be reached in a depth of acquisition lower than 90 mm with clinically available ultrasounds. This alternative can be implemented in the clinical setting more easily than parallel beamforming techniques available on more expensive hardware (Jensen et al., 2013; Kaczkowski and Daigle, 2011).

Magnetic excitation lasting for a single cycle suffices to locate the magnetic particles and generate broadband SW. In a single-cycle configuration, tracking the ultrasound for a $T_{US} = 50$ ms is sufficient to analyze MMUS and SDMMUS. Furthermore, the multiple reflections of the shear wave (which occur in the phantom walls) decrease and the overall acquisition time diminishes as compared to harmonic excitation (Almeida et al, 2015).

According to (Oudry et al., 2009) the elastic property of a linear, isotropic, and incompressible material is related to the shear storage modulus μ . This approach gives $\mu = 14095$ kPa and Young's modulus of 42285 kPa, calculated by using $c_g = 4.17$ m/s. These values are comparable to the dynamic method described by (Vieira et al., 2013). However, studies have already demonstrated that biological tissues are viscoelastic materials (Sarvazyan et al., 2013). Considering paraffin as a viscoelastic material, we must use the complex shear modulus $\mu = \mu_1 + j\mu_2$ of the Kelvin-Voigt model, which employs the phase velocity and attenuation coefficient as input parameters to obtain elasticity and viscosity, i.e., μ_1 and μ_2 , respectively. Gaussian filter analysis (Parolai, 2009) can be applied to estimate the attenuation coefficient and the phase velocity, to give $\mu_1 = 5.05$ kPa and $\mu_2 = 2.01$ Pa.s at a frequency of 100 Hz. This provides faster and easier frequency dispersion analysis than harmonic excitation (Almeida et al., 2015). However, using magnetic excitation that lasts longer than one

cycle facilitates ROE segmentation, which can be improved by applying a relative energy threshold of 30% to 50%. This improvement can help to segment a region containing a high concentration of particles that are probably aggregated.

Finally, this paper has presented a software-based platform for MMUS applications that provides an easy-to-use MMUS interface and allows quick configuration for MMUS or SDMMUS. Moreover, addressing a default preset will help future applications in the clinical setting without losing the flexibility of the MMUS system. Future works should continue the development of this platform to provide real-time MMUS/SDMMUS at low cost and focus on different applications such as the mechanical characterization of tissues, which lead to implement a new clinical MMUS imaging modality.

Acknowledgements

We acknowledge FINEP (MCT2613/09), CAPES, CNPq, and FAPESP (2010/07639-9; 2012/18420-3; 2013/18854-6) for financial support. We also thank Gphantom for helping to produce tissue-mimicking samples.

References

- Almeida TWJ, Sampaio DRT, Bruno AC, Pavan TZ, Carneiro AAO. Comparison between shear wave dispersion magneto motive ultrasound and transient elastography for measuring tissue-mimicking phantom viscoelasticity. *IEEE Transactions on Ultrasonics, Ferroelectrics, and Frequency Control*. 2015; 62(12):2138-45. PMID:26670853. <http://dx.doi.org/10.1109/TUFFC.2015.007353>.
- Almeida TWJ, Sampaio DRT, Pavan TZ, Carneiro AAO. Shear wave Vibro Magneto Acoustography for measuring tissue mimicking phantom elasticity and viscosity. In: 2014 IEEE International Ultrasonics Symposium (IUS); 2014. USA: IEEE; 2014. p. 1097-100. <http://doi.org/10.1109/ULTSYM.2014.0269>.
- Bruno AC, Sampaio DRT, Pavan TZ, Baffa O, Carneiro AAO. A hybrid transducer to evaluate stomach emptying by ultrasound and susceptometric measurements: an in vivo feasibility study. *IEEE Transactions on Ultrasonics, Ferroelectrics, and Frequency Control*. 2015; 62(7):1288-94. PMID:26168175. <http://dx.doi.org/10.1109/TUFFC.2014.006950>.
- Cobbold RSC. *Foundations of biomedical ultrasound*. Oxford: Oxford University Press; 2006.
- Colello Bruno A, Baffa O Fo, Carneiro AAO, Oliveira RB. Stomach emptying evaluation by ultrasound and susceptometric measurements with a hybrid transducer. In: 2014 IEEE International Ultrasonics Symposium (IUS); 2014. USA: IEEE; 2014. p. 1869-72. <http://doi.org/10.1109/ULTSYM.2014.0464>.
- Colello Bruno A, Pavan TZ, Baffa O, Oliveira Carneiro AA. A hybrid transducer to magnetically and ultrasonically evaluate magnetic fluids. *IEEE Transactions on Ultrasonics, Ferroelectrics, and Frequency Control*. 2013; 60(9):2004-12. PMID:24658731. <http://dx.doi.org/10.1109/TUFFC.2013.2785>.
- Deffieux T, Montaldo G, Tanter M, Fink M. Shear Wave Spectroscopy for In Vivo Quantification of Human Soft Tissues Visco-Elasticity. *IEEE Transactions on Medical Imaging*. 2009; 28(3):313-22. PMID:19244004. <http://dx.doi.org/10.1109/TMI.2008.925077>.
- Evertsson M, Kjellman P, Cinthio M, Fredriksson S, in't Zandt R, Persson H, Jansson T. Multimodal detection of iron oxide nanoparticles in rat lymph nodes using magnetomotive ultrasound imaging and magnetic resonance imaging. *IEEE Transactions on Ultrasonics, Ferroelectrics, and Frequency Control*. 2014; 61(8):1276-83. PMID:25073135. <http://dx.doi.org/10.1109/TUFFC.2014.3034>.
- Hemmsen MC, Nikolov SI, Pedersen MM, Pihl MJ, Enevoldsen MS, Hansen JM, Jensen JA. Implementation of a versatile research data acquisition system using a commercially available medical ultrasound scanner. *IEEE Transactions on Ultrasonics, Ferroelectrics, and Frequency Control*. 2012; 59(7):1487-99. PMID:22828844. <http://dx.doi.org/10.1109/TUFFC.2012.2349>.
- Jensen JA, Holten-Lund H, Nilsson RT, Hansen M, Larsen UD, Domsten RP, Tomov BG, Stuart MB, Nikolov SI, Pihl MJ, Yigang Du, Rasmussen JH, Rasmussen MF. SARUS: a synthetic aperture real-time ultrasound system. *IEEE Transactions on Ultrasonics, Ferroelectrics, and Frequency Control*. 2013; 60(9):1838-52. PMID:24658717. <http://dx.doi.org/10.1109/TUFFC.2013.2770>.
- Jin Y, Jia C, Huang S-W, O'Donnell M, Gao X. Multifunctional nanoparticles as coupled contrast agents. *Nature Communications*. 2010; 1(4):41. PMID:20975706. <http://dx.doi.org/10.1038/ncomms1042>.
- Kaczkowski PJ, Daigle RE. The Verasonics ultrasound system as a pedagogic tool in teaching wave propagation, scattering, beamforming, and signal processing concepts in physics and engineering. *The Journal of the Acoustical Society of America*. 2011; 129(4):2648. <http://dx.doi.org/10.1121/1.3588831>.
- Liu D, Ebbini ES. Real-time 2-D temperature imaging using ultrasound. *IEEE Transactions on Biomedical Engineering*. 2010; 57(1):12-6. PMID:19884075. <http://dx.doi.org/10.1109/TBME.2009.2035103>.
- McAleavey SA, Rubens DJ, Parker KJ. Doppler ultrasound imaging of magnetically vibrated brachytherapy seeds. *IEEE Transactions on Biomedical Engineering*. 2003; 50(2):252-5. PMID:12665040. <http://dx.doi.org/10.1109/TBME.2002.807644>.
- Mehrmohammadi M, Oh J, Mallidi S, Emelianov SY. Pulsed magneto-motive ultrasound imaging using ultrasmall magnetic nanoprobles. *Molecular Imaging*. 2011a; 10(2):102-10. PMID:21439255.
- Mehrmohammadi M, Qu M, Ma LL, Romanovicz DK, Johnston KP, Sokolov KV, Emelianov SY. Pulsed magneto-motive ultrasound imaging to detect intracellular

- trafficking of magnetic nanoparticles. *Nanotechnology*. 2011b; 22(41):415105. PMID:21926454. <http://dx.doi.org/10.1088/0957-4484/22/41/415105>.
- Mehrmohammadi M, Yoon KY, Qu M, Johnston KP, Emelianov SY. Enhanced pulsed magneto-motive ultrasound imaging using superparamagnetic nanoclusters. *Nanotechnology*. 2011c; 22(4):045502. PMID:21157009. <http://dx.doi.org/10.1088/0957-4484/22/4/045502>.
- Oh J, Feldman MD, Kim J, Condit C, Emelianov S, Milner TE. Detection of magnetic nanoparticles in tissue using magneto-motive ultrasound. *Nanotechnology*. 2006; 17(16):4183-90. PMID:21727557. <http://dx.doi.org/10.1088/0957-4484/17/16/031>.
- Oudry J, Chen J, Glaser KJ, Miette V, Sandrin L, Ehman RL. Cross-validation of magnetic resonance elastography and ultrasound-based transient elastography: a preliminary phantom study. *Journal of Magnetic Resonance Imaging*. 2009; 30(5):1145-50. PMID:19856447. <http://dx.doi.org/10.1002/jmri.21929>.
- Parolai S. Determination of dispersive phase velocities by complex seismic trace analysis of surface waves (CASW). *Soil Dynamics and Earthquake Engineering*. 2009; 29(3):517-24. <http://dx.doi.org/10.1016/j.soildyn.2008.05.008>.
- Pavan TZ, Sampaio DRT, Carneiro AAO, Covas DT. Ultrasound-based transient elastography using a magnetic excitation. In: 2012 IEEE International Ultrasonics Symposium (IUS); 2012. USA: IEEE; 2012. p. 1846-9. <http://doi.org/10.1109/ULTSYM.2012.0463>.
- Qt. Qt cross-plaform framework [internet]. Santa Clara: Qt; 2016 [cited 2016 Apr 29]. Available from: <http://www.qt.io/developers/>
- Qu M, Mallidi S, Mehrmohammadi M, Truby R, Homan K, Joshi P, Chen YS, Sokolov K, Emelianov S. Magneto-photo-acoustic imaging. *Biomedical Optics Express*. 2011; 2(2):385-96. PMID:21339883. <http://dx.doi.org/10.1364/BOE.2.000385>.
- Sarvazyan AP, Urban MW, Greenleaf JF. Acoustic waves in medical imaging and diagnostics. *Ultrasound in Medicine & Biology*. 2013; 39(7):1133-46. PMID:23643056. <http://dx.doi.org/10.1016/j.ultrasmedbio.2013.02.006>.
- Shamdasani V, Bae U, Sikdar S, Yoo YM, Karadayi K, Managuli R, Kim Y. Research interface on a programmable ultrasound scanner. *Ultrasonics*. 2008; 48(3):159-68. PMID:18234260. <http://dx.doi.org/10.1016/j.ultras.2007.11.009>.
- Urban MW, Chalek C, Kinnick RR, Kinter TM, Haider B, Greenleaf JF, Thomenius KE, Fatemi M. Implementation of vibro-acoustography on a clinical ultrasound system. *IEEE Transactions on Ultrasonics, Ferroelectrics, and Frequency Control*. 2011; 58(6):1169-81. PMID:21693399. <http://dx.doi.org/10.1109/TUFFC.2011.1927>.
- Vieira SL, Pavan TZ, Junior JE, Carneiro AAO. Paraffin-gel tissue-mimicking material for ultrasound-guided needle biopsy phantom. *Ultrasound in Medicine & Biology*. 2013; 39(12):2477-84. PMID:24035622. <http://dx.doi.org/10.1016/j.ultrasmedbio.2013.06.008>.
- Viola F, Walker WF. A spline-based algorithm for continuous time-delay estimation using sampled data. *IEEE Transactions on Ultrasonics, Ferroelectrics, and Frequency Control*. 2005; 52(1):80-93. PMID:15742564. <http://dx.doi.org/10.1109/TUFFC.2005.1397352>.
- Wilson T, Zagzebski J, Varghese T, Chen Q, Rao M. The Ultrasonix 500RP: a commercial ultrasound research interface. *IEEE Transactions on Ultrasonics, Ferroelectrics, and Frequency Control*. 2006; 53(10):1772-82. PMID:17036786. <http://dx.doi.org/10.1109/TUFFC.2006.110>.
- Zahiri-Azar R, Baghani A, Salcudean SE, Rohling R. 2-D high-frame-rate dynamic elastography using delay compensated and angularly compounded motion vectors: preliminary results. *IEEE Transactions on Ultrasonics, Ferroelectrics, and Frequency Control*. 2010; 57(11):2421-36. PMID:21041130. <http://dx.doi.org/10.1109/TUFFC.2010.1709>.
- Zahiri-Azar R, Salcudean SE. Motion estimation in ultrasound images using time domain cross correlation with prior estimates. *IEEE Transactions on Biomedical Engineering*. 2006; 53(10):1990-2000. PMID:17019863. <http://dx.doi.org/10.1109/TBME.2006.881780>.
- Zhao H, Urban M, Greenleaf J, Chen S. Elasticity and viscosity estimation from shear wave velocity and attenuation: a simulation study. In: 2010 IEEE International Ultrasonics Symposium (IUS); 2010. USA: IEEE; 2010. p. 1604-7. <http://doi.org/10.1109/ULTSYM.2010.5935462>.

Authors

Diego Ronaldo Thomaz Sampaio^{1*}, Felipe Wilker Grillo¹, Alexandre Colello Bruno¹, Theo Zeferino Pavan¹, Antonio Adilton Oliveira Carneiro¹

¹ Department of Physics, Faculty of Philosophy, Science and Letters of Ribeirão Preto, Universidade de São Paulo – USP, Av. Bandeirantes, 3900, Bairro Monte Alegre, CEP 14040-901, Ribeirão Preto, SP, Brazil.